Journal of Materials Chemistry

Cite this: J. Mater. Chem., 2012, 22, 5587

www.rsc.org/materials

PAPER

Improved thin film morphology and bulk-heterojunction solar cell performance through systematic tuning of the surface energy of conjugated polymers†

Ying Sun,[ab] Shang-Chieh Chien,[ac] Hin-Lap Yip,[a] Kung-Shih Chen,[a] Yong Zhang,[a] Joshua A. Davies,[a] Fang-Chung Chen,[c] Baoping Lin*[b] and Alex K.-Y. Jen*[a]

Received 28th October 2011, Accepted 6th January 2012
DOI: 10.1039/c2jm15517f

A detailed model study has shown that thin film morphology and bulk-heterojunction solar cell performance can be significantly improved by systematic tuning of the surface energy of the conjugated donor polymer through side-chain functionalization. Thiophene-flanked diketopyrrolopyrrole (DPP) moieties with different contents of cyanohexane side chains were incorporated into three low band-gap conjugated copolymers (**PIDTDPP1**, **PIDTDPP2** and **PIDTDPP3**) consisting of indacenodithiophene (IDT) donors and DPP acceptors. The resulting polymers possessed good solubility in common organic solvents and showed similar energy levels, bandgaps, and hole mobilities. However, the introduction of cyano groups onto the terminal of side-chains significantly changed their surface energy. Topographical images obtained from atomic force microscopy (AFM) proved that a better matched surface energy between polymer and $PC_{71}BM$ had led to enhanced miscibility, which resulted in better BHJ film morphology. Consistent with the surface energy enhancement, the performance of BHJ photovoltaic devices increased from 0.97% for **PIDTDPP1**, to 2.16% for **PIDTDPP2** then to 3.67% for **PIDTDPP3**. These results clearly reveal that tuning surface energy is an effective way to improve the morphology of the BHJ active layer and efficiency of the photovoltaic device.

Introduction

In the past decade, progress in the area of polymer solar cells (PSCs) has shown that they have great potential to be used as low-cost, flexible, and light-weight renewable energy sources. The performance of bulk-heterojunction (BHJ) based PSCs has reached more than 7–8% in power conversion efficiency (PCE) by carefully tailoring the energy level and bandgap of conjugated polymers and fullerene derivatives.[1–9]

The film morphology of the BHJ active layer plays a significant role in determining the effectiveness of exciton dissociation and charge transport, hence, the overall PSC efficiency.[10–13] Due to the relatively high exciton binding energy (~0.3 to 0.5 eV) and short exciton diffusion length (~10 nm) in conjugated polymers, a large donor/acceptor interfacial area is required in order to have efficient exciton dissociation into free charge carriers.[14] However, if the scale of phase separation (domain size) is smaller than the Coulomb capture radius, it will also increase the chance for geminate or bimolecular recombination.[14–16] Therefore, an optimum film morphology in the BHJ layer is very critical for efficient charge dissociation, as well as for providing a nanoscale bicontinuous pathway for better charge transport with minimized charge recombination.[14]

Most recent efforts to optimize the BHJ film morphology have been focused on manipulating device processing conditions in terms of coating solvent, additive, blending ratio, annealing treatment and substrate surface control.[12,17–21] In spite of the improved performance, the processing conditions vary significantly between different material systems and it is painstaking to individually optimize. Very few general guidelines can be applied to the process optimization to predict and obtain good film morphology. In addition, this processing optimization definitely increases the device fabrication complexity and reduces the reproducibility, which is not beneficial for large-scale manufacturing.

BHJ film morphology mostly relies upon the miscibility between the donor and acceptor molecules,[22,23] which is strongly associated with the surface energy of blending components.[14,16,24] Recently, Kim *et al.* have successfully tuned the film morphology of a P3HT/PCBM BHJ layer by changing the surface energy of

[a]*Department of Materials Science and Engineering, University of Washington, Seattle, Washington, 98195, USA. E-mail: ajen@u.washington.edu; Fax: +1 206 543 3100; Tel: +1 206 543 2626*
[b]*School of Chemistry and Chemical Engineering, Southeast University, Jiangning District, Nanjing, Jiangsu Province, P.R. China 211189. E-mail: lbp@seu.edu.cn; Fax: +86-25-52090616; Tel: +86-25-52090616*
[c]*Department of Photonics & Display Institute, National Chiao Tung University, Hsinchu 30010, Taiwan*
† Electronic supplementary information (ESI) available. See DOI: 10.1039/c2jm15517f

lower molecular weight P3HT *via* end-group modification.[24] They have demonstrated that good miscibility and blending homogeneity in film could be achieved when the active layer components had a similar surface energy. The well-controlled phase separation in both the vertical and horizontal directions has led to reduced series resistance, enhanced fill factor, and better device performance. This result is very encouraging, however, there has been very little research conducted on tuning the surface energy of high molecular weight, low bandgap polymers.

Recently, diketopyrrolopyrrole (DPP)-based polymers have been extensively investigated in the context of field-effect transistors (FETs) and organic photovoltaic (OPV) cells due to their dual advantages of superior optical properties and excellent charge carrier mobilities as a result of strong π–π interactions and good backbone planarity.[22,25–31] By varying the donor segments, it has afforded a series of donor–acceptor polymers showing extraordinary hole mobilities with the highest value of ~2 $cm^2 V^{-1} s^{-1}$ and the best photovoltaic device performance of over 5.5%.[25–28] However, most of the DPP based polymers encounter the problem of low miscibility with fullerene derivatives and need to be processed with the aid of additives to achieve desired film morphologies.[26,27,32]

In this paper, we introduce a simple and generally applicable method to manipulate the surface energy of high molecular weight, low bandgap polymers. In particular, the utilization of structure modification to influence BHJ film morphology is highlighted. A new alternating copolymer **PIDTDPP1** was synthesized initially by incorporating the indacenodithiophene (IDT) donor unit with the ethylhexyl-substituted DPP acceptor. The IDT unit features a fused ring aromatic structure containing two thiophene rings rigidified with a phenyl group that can offer strong intermolecular interactions to afford ordered molecular organization.[33–35] Afterward, the side-chains of the DPP moiety were modified with cyano groups and then were introduced into polymer chains, yielding two new copolymers **PIDTDPP2** and **PIDTDPP3** with different contents of cyano functionalized DPP units (CNDPP). The cyano group can be easily introduced to the terminal of side chains by employing 6-bromohexanenitrile to react with the unsubstituted bis-thiophen-2-yl-DPP moiety. The high polarity of the cyano group will help increase the surface energy while its small size will not introduce any potential steric hindrance.

The flexibility of tuning CNDPP content in the polymer through changing the monomer ratio in the copolymerization allowed us to easily control the polar characteristics of polymer and surface energy. The results from cyclic voltammetry and organic field-effect transistor (OFET) measurements showed that these three polymers **PIDTDPP1**, **PIDTDPP2** and **PIDTDPP3** have similar energy levels and hole mobilities, which enable us to differentiate the surface energy effect from other factors that may potentially influence device performance. Surface energy, measured from contact angle analysis, was determined to be 30.2, 31.9 and 34.8 mN m^{-1} for **PIDTDPP1**, **PIDTDPP2** and **PIDTDPP3**, respectively. When the surface energy of the polymer was tuned to be close to that of $PC_{71}BM$ (34.3 mN m^{-1}), better miscibility occurred, resulting in an optimized BHJ morphology and significantly improved photovoltaic device performance. The PCE increased from 0.97% for **PIDTDPP1** to 2.16% for **PIDTDPP2** to 3.67% for **PIDTDPP3**. This approach is unique compared to previous approaches described in the literature. In this paper, we have modified the low bandgap polymer through simple functionalization of side-chains to improve the morphology of the BHJ film rather than adding a separate additive material. Additionally, this work has enabled us to better understand the relationships between polymer chemical structure, physical properties, BHJ film morphology, and photovoltaic performance.

Results and discussion

Synthesis

The solubility of the monomer is very critical for the resulting polymer to achieve good solution processability and high molecular weight.[36] The diketopyrrolopyrrole moiety consisting of two highly conjugated fused aromatic rings has low solubility in common solvents due to its strong intermolecular H-bonding. To ensure good solubility of targeted polymers, a branched alkyl chain and a cyanohexyl side-chain were introduced onto the DPP backbone. Scheme 1 illustrates the synthetic routes for making the cyano functionalized DPP monomer **3**. At first, the unsubstituted bis-thiophen-2-yl-DPP compound **1** was treated with 2.6 equivalents of 1-bromo-6-cyanohexane and 3.3 equivalents of potassium carbonate (K_2CO_3) in DMF, giving compound **2** with 67% yield. After this, NBS bromination provided the target monomer compound **3**. The donor IDT monomer **5** and 3,6-bis-(5-bromothiophen-2-yl)-2,5-di-2-ethylhexyl-pyrrolo[3,4-*c*]pyrrole-1,4-dione **4** were synthesized according to the reported procedures.[34,37]

The synthetic approaches for making the polymers are depicted in Scheme 2. Stille coupling polymerizations between the IDT donor monomer **5** and the DPP acceptors **3** and **4** yielded three polymers by using $Pd_2(dba)_3$ and ligand P(*o*-tol)$_3$ as the catalyst. The content of cyano functionalized DPP units was carefully controlled to tune the polarity of polymers. The resulting polymers were first washed by Soxhlet extraction using acetone and hexane. They were further purified by dissolving in $CHCl_3$ or chlorobenzene and then slowly precipitated in hexane. The chemical structures of the polymers were characterized by using ^{1}H NMR. We also investigated the thermal properties of the polymers with differential scanning calorimetry (DSC) but no thermal transitions could be observed in the temperature range between 20 and 350 °C for all the three polymers (see ESI†).

The molecular weight of the polymers was determined by gel permeation chromatography (GPC) against the polystyrene standard with THF used as the eluent. The detailed GPC data

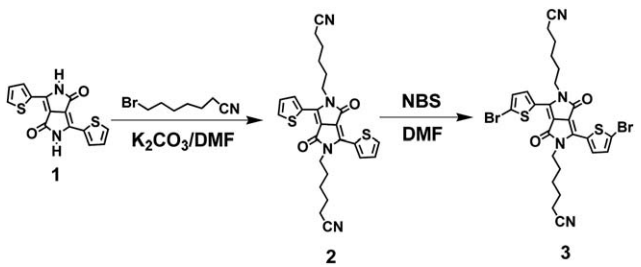

Scheme 1 Synthetic routes for the cyano functionalized monomer.

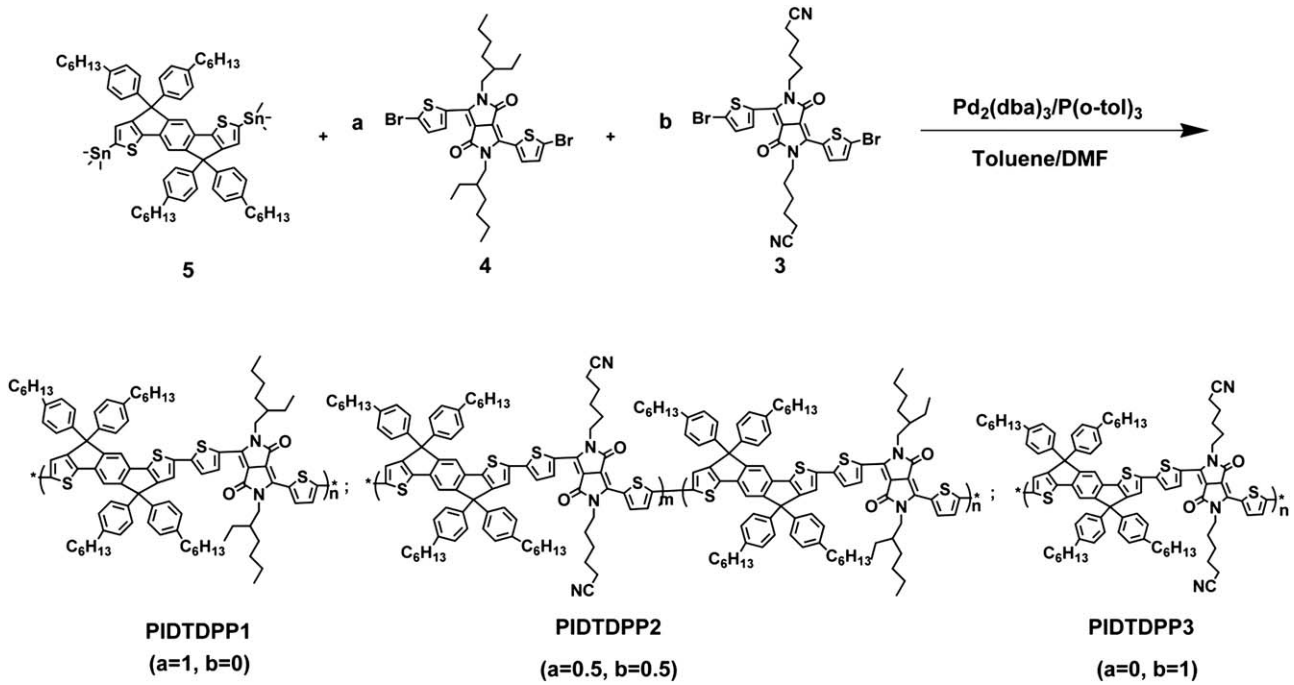

Scheme 2 Synthetic routes for the polymers.

are listed in Table 1. All three polymers have good solubility in chloroform ($CHCl_3$), chlorobenzene (CB) and dichlorobenzene (DCB), especially for **PIDTDPP1** and **PIDTDPP2**. Therefore we can explore the influencing factors of the device performance without considering the solubility effect related to side chain modification and polymer molecular weight differences.

Optical and electrochemical properties

The normalized UV-vis absorption spectra of the polymers both in $CHCl_3$ and in films are shown in Fig. 1. All three polymers showed two similar absorption bands in the range of 350–450 nm and 550–800 nm. While the first, higher energy peak can be attributed to the π–π* transition originating from the conjugated polymer chain, the second peak may arise from the intramolecular charge transfer (ICT) transition between donor IDT and acceptor DPP units.[36] No obvious differences in the absorption maxima between polymers in solution and in film can be observed, possibly suggesting a strong intermolecular interaction of polymer chains in both solution and film. However, **PIDTDPP3** showed a red-shifted absorption maximum in the film by 10 nm compared to **PIDTDPP1** and **PIDTDPP2**. This may be due to the higher degree of aggregation from the more polar polymer side-chains in the solid state. The optical bandgap calculated from the onset of absorption spectra was estimated to be 1.59, 1.58, and 1.56 eV for **PIDTDPP1**, **PIDTDPP2** and **PIDTDPP3**, respectively. The similar bandgaps for these three polymers indicate that the change of the alkyl chain to the cyano substituted side-chain had no distinct effect on electron delocalization within the conjugated system.

The electrochemical properties of the polymers were investigated by employing cyclic voltammetry. Fig. 2 shows the cyclic voltammograms which were measured using a Pt counter electrode and an Ag/Ag^+ reference electrode in an 0.1 M electrolyte containing tetrabutylammonium hexafluoro-phosphate in acetonitrile with a scan rate of 100 mV s^{-1}. HOMO and LUMO levels of polymers were calculated using the following equation:

$$\text{HOMO} = -[E_{ox} + 4.80]\ \text{eV};\ \text{LUMO} = -[E_{red} + 4.80]\ \text{eV}$$

in which E_{ox} and E_{red} are the onset of the oxidation and reduction potential, respectively. The HOMO levels were determined to be around −5.16 eV to −5.19 eV and the LUMO levels were calculated to be around −3.20 eV for three polymers.

Table 1 Molecular weights, optical, and electrochemical properties and OFET device results of polymers

			UV-vis absorption				Cyclic voltammetry					
			In $CHCl_3$		In film							
Polymer	M_n/ kg mol^{-1}	PDI	λ_{max}/ nm	λ_{onset}/ nm	λ_{max}/ nm	λ_{onset}/ nm	HOMO/ eV	LUMO/ eV	Band gap/ eV	Hole mobility/ $cm^2\ V^{-1}\ s^{-1}$	Threshold voltage/V	On/off ratio
PIDTDPP1	65.1	2.27	721	795	721	782	−5.16	−3.18	1.59	0.015	−6	10^5
PIDTDPP2	65.8	2.92	721	779	721	791	−5.19	−3.20	1.58	0.0072	4	10^4
PIDTDPP3	98.0	2.90	735	779	735	797	−5.18	−3.23	1.56	0.011	−26	10^4

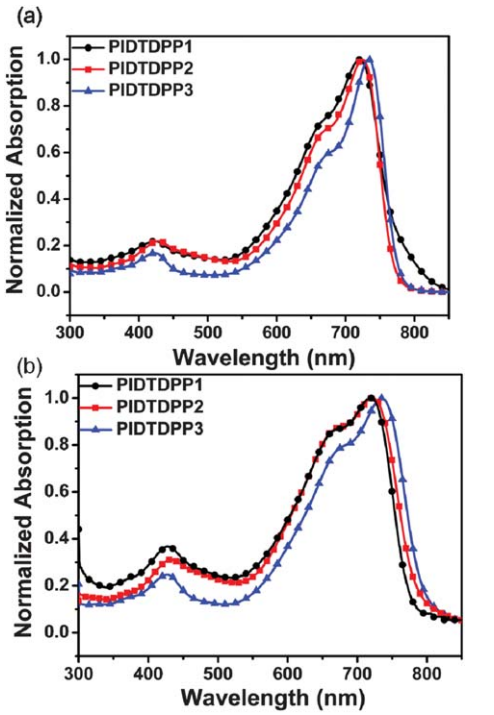

Fig. 1 UV-vis absorption spectra of the polymers in (a) chloroform and (b) thin film.

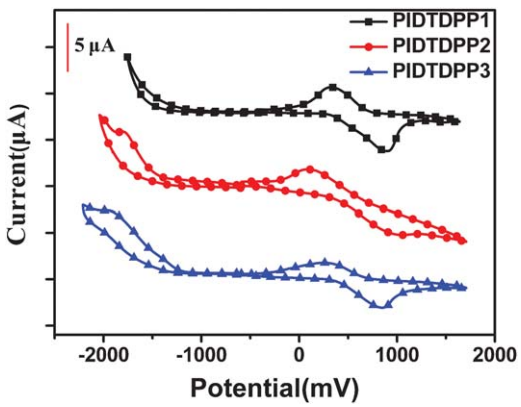

Fig. 2 Cyclic voltammogram of polymers (scan rate: 100 mV s^{-1}).

The detailed results are summarized in Table 1. These results indicate that side chain modifications give rise to negligible effects on the energy levels of the polymers, which allows us to determine the effect of the surface energy change on the BHJ device performance and easily distinguish it from other influencing factors.

Field-effect mobility measurements

The charge carrier mobility of the polymer is very critical for BHJ photovoltaic device performance as it is directly related to the efficiency of charge transport and collection.[38,39] Therefore, it is essential to study the effect of functionalization of cyano containing side-chains on the hole mobilities of polymers. Organic field-effect transistor (OFET) devices derived from these polymers were fabricated using a bottom-gate, top-contact configuration to investigate field-effect mobility of the polymers. Fig. 3 shows the output curves under different gate voltages (V_{gs}) and transfer characteristics in the saturation regime using constant source–drain voltage ($V_{ds} = -100$ V) for these three polymers. From the results, all three polymers showed the typical p-type FET characteristics with hole mobility determined to be 0.015 cm^2 V^{-1} s^{-1}, 0.0072 cm^2 V^{-1} s^{-1} and 0.011 cm^2 V^{-1} s^{-1} for polymers **PIDTDPP1**, **PIDTDPP2** and **PIDTDPP3**, respectively, while the on/off ratio was on the order of 10^4 to 10^5 (Table 1).

The relatively high mobility of these polymers suggests that they have well-defined structure organization and strong intermolecular interactions as a result of the planar fused ring system of the IDT and DPP units.[28,31] The introduction of cyano groups onto the side-chains has led to a negligible change in mobility as **PIDTDPP3** showed a mobility comparable to **PIDTDPP1**. Compared to the other two polymers, the decreased mobility for **PIDTDPP2** may be due to a less ordered structural organization in its regio-random structure.

Photovoltaic properties

Surface properties of the individual components in the BHJ layer are very critical in determining their compatibility in the blend. Since the surface energy of a material is related to its polarity, crystallinity, and surface interactions, contact angle tests were performed on polymer films to investigate the effect of cyano-containing side-chains on the surface energy of the polymers. As expected, the increased content of CNDPP units on polymer chains led to higher surface energy value which is 34.8 mN m^{-1} for **PIDTDPP3** and 31.9 mN m^{-1} for **PIDTDPP2** compared to 30.2 mN m^{-1} for **PIDTDPP1**. The surface energy of $PC_{71}BM$ was also measured to be 34.3 mN m^{-1} which is close to the reported value for $PC_{61}BM$.[40] The calculation method[41] and experimental data for the contact angle, dispersive and polar surface energy components for polymers and $PC_{71}BM$ are summarized in the ESI†.

We speculate that the closer surface energy of the individual components in a BHJ should facilitate better miscibility, which will lead to a more homogeneously mixed blend. To correlate the film morphology with surface energy, the BHJ layer from three polymers was spin-coated on top of poly(3,4-ethylenedioxythiophene):poly(styrenesulfonate) (PEDOT:PSS)-coated indium tin oxide (ITO) glasses from their dichlorobenzene solutions of polymer and $PC_{71}BM$ with a 1 : 3 (w/w) ratio.

Fig. 4 illustrates the atomic force microscopy (AFM) height images and surface profiles of BHJ films. The AFM image of **PIDTDPP1** showed serious coarse-grained phase separation with a surface roughness of 4.24 nm measured from its height image. This coarse surface morphology is probably due to the low entropy of mixing between the polymer and $PC_{71}BM$ since immiscible materials tend to phase segregate into large domains during the spin-coating process.[42] With a higher surface energy, polymer **PIDTDPP2** showed a decreased phase separation and a smaller surface roughness of 3.15 nm. For **PIDTDPP3**, the surface morphology is quite smooth and homogeneous with a surface roughness of around 0.90 nm. The obvious trend of film morphology change can also be clearly observed from the surface profile results.

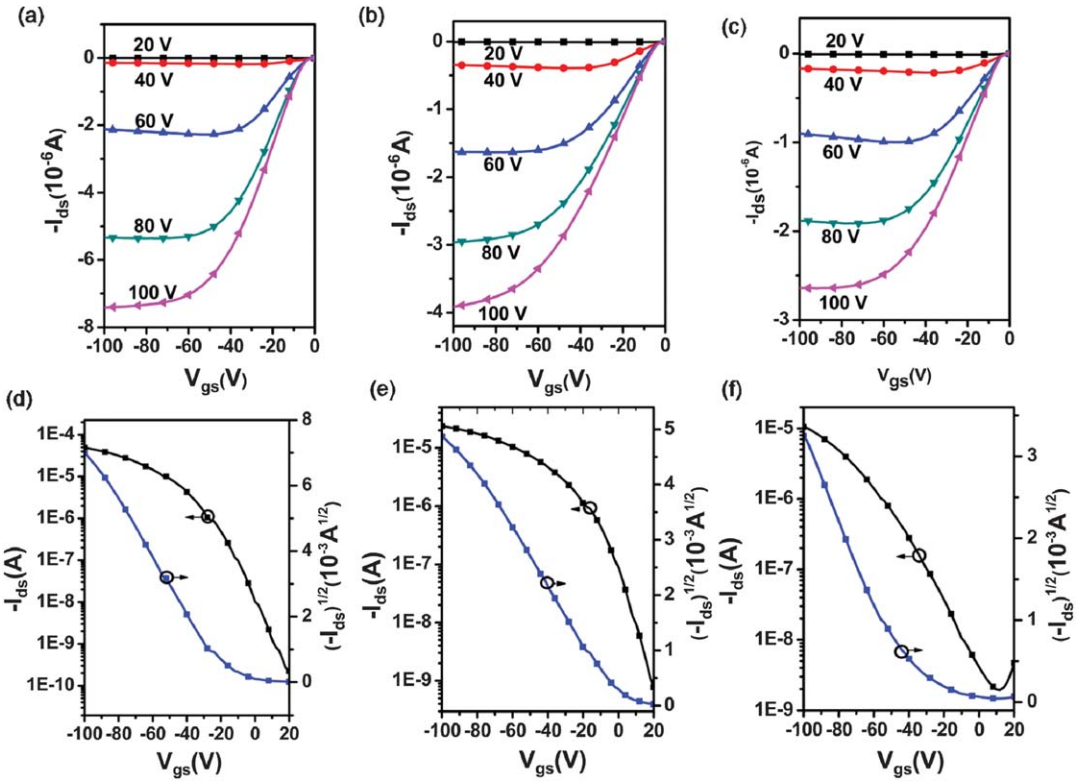

Fig. 3 OFET characteristics of polymers. Output (a–c) and transfer (d–f) characteristics of **PIDTDPP1** (a and d), **PIDTDPP2** (b and e) and **PIDTDPP3** (c and f).

The systematically improved morphology shows that surface energy can play a crucial role in enhancing the miscibility of components in a blend and that the closer surface energy can potentially result in better film morphology, which is expected to increase the interfacial D–A area for more efficient charge generation and dissociation.[7,15]

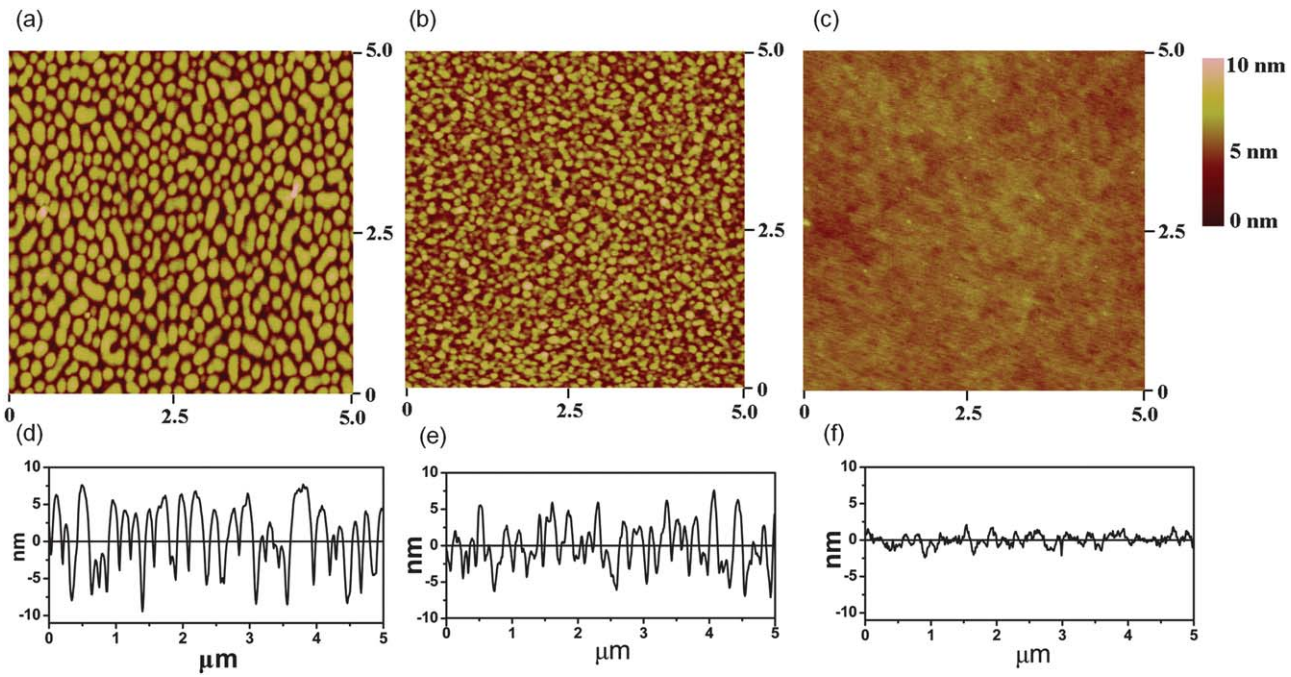

Fig. 4 Tapping mode AFM height images (a–c) and surface profiles (d–f) of the films based on polymers **PIDTDPP1** (a and d), **PIDTDPP2** (b and e) and **PIDTDPP3** (c and f) with $PC_{71}BM$ (1 : 3).

Photovoltaic properties of these polymers were investigated in BHJ PSCs using a device configuration of ITO/PEDOT:PSS (40 nm)/polymer:$PC_{71}BM$/Ca (30 nm)/Al (100 nm). The device area was defined to be 10.08 mm^2 with a mask and the detailed fabrication procedures are described in the Experimental section. $PC_{71}BM$ was chosen as the acceptor due to its broader absorption around 500 nm, which is complementary to the low bandgap polymer. The weight ratio between the donor polymer and $PC_{71}BM$ was optimized to be 1 : 3 in order to achieve the best performance for all three polymers. The representative *J–V* characteristics of BHJ PSCs recorded under the AM 1.5 G simulated solar illumination with an incident power density of 100 mW cm^{-2} are illustrated in Fig. 5(a) and the detailed performance parameters are summarized in Table 2.

The photovoltaic device based on the **PIDTDPP1**:$PC_{71}BM$ active layer (100 nm) showed a V_{oc} of 0.76 V, a J_{sc} of 2.63 mA cm^{-2}, and a FF of 0.47, yielding an optimal PCE of only 0.95%. This poor device performance can be correlated to the coarse film morphology where the phase separated domain size is too large to achieve efficient exciton dissociation. Considering the limited exciton diffusion length of the organic conjugated polymer, most of the generated excitons probably cannot reach the donor–acceptor interfaces to dissociate into free charge carriers within their lifetime. For polymer **PIDTDPP2**, the BHJ device showed a significantly improved J_{sc} of 5.64 mA cm^{-2} while the V_{oc} and FF increased slightly compared to **PIDTDPP1**.

In the case of polymer **PIDTDPP3**, an even higher J_{sc} of 9.80 mA cm^{-2} could be achieved while its V_{oc} and FF remain similar to those of **PIDTDPP1**. The result of significantly enhanced J_{sc} showed that better film morphology facilitates more efficient charge dissociation and transport in BHJ active layers, which leads to higher device performance.

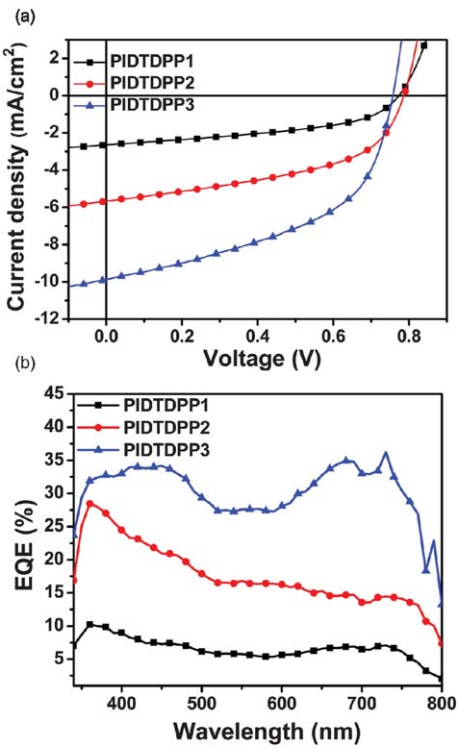

Fig. 5 *J–V* curves (a) and EQE (b) of optimized bulk heterojunction solar cells based on polymers and $PC_{71}BM$ (1 : 3 (w/w)).

In addition to *J–V* characteristics, the external quantum efficiencies (EQEs) of the devices based on the blends of three polymers and $PC_{71}BM$ were measured and the EQE spectra are recorded in Fig. 5(b). The EQE spectra of the active blending layer in devices are consistent with the observed film morphological changes and photocurrent enhancements. The **PIDTDPP1** based device showed a low photo-response value of less than 10% between 350 and 800 nm, while the highest EQE value increased to 28% for **PIDTDPP2**. The device consisting of **PIDTDPP3**:$PC_{71}BM$ BHJ yielded an EQE greater than 20% between 350 and 750 nm, and a higher value of 36% at ~730 nm. The enhanced J_{sc} in conjunction with the EQE change is a clear indication of an improved charge photo-generation and efficient charge transfer corresponding to the better film morphology.

Thereby, the results from these measurements strongly support our concept of manipulating the surface energy of the polymer to enhance its compatibility with $PC_{71}BM$ for improved BHJ PSCs device performance. Moreover, it is generally acknowledged that V_{oc} is mainly determined by the energy difference between the HOMO level of the polymer and the LUMO level of the acceptor when the Ohmic contact at the electrode/BHJ interfaces can be achieved.[36] The negligible variation in V_{oc} for three polymers also confirmed the previous discussion that our functionalization of the side-chains does not introduce notable effects on the energy level alignment of the polymers.

The above discussion indicates a clear relationship between surface energy, BHJ film morphology and photovoltaic device performance. In this respect, we offer a promising tool to aid rational material design for enhanced device performance. As yet, the present study is only focused on the correlation between the BHJ lateral film morphology and device performance with surface energy matching. Further investigations are in progress to explore the effect of varying surface energy properties on other factors that influence PSCs device performance.

Conclusion

We report that tuning surface energy can be an effective tool to improve the miscibility between conjugated polymer donors and fullerene derivatives for optimizing the BHJ film morphology. Three model low bandgap copolymers **PIDTDPP1**, **PIDTDPP2** and **PIDTDPP3** consisting of IDT and DPP units have been synthesized to possess systematically tuned polar characteristics through the functionalization of cyano groups on the side-chains. The HOMO and LUMO energy levels of these polymers are quite similar and the cyanohexyl-functionalized copolymers also possess comparable hole mobility. The surface energy obtained from contact angle measurements of these polymers is 30.2, 31.9 and 34.8 mN m^{-1} for **PIDTDPP1**, **PIDTDPP2** and **PIDTDPP3**, respectively. The results from AFM images indicate a close correlation between the film morphology and surface energy. A relatively smooth film was achieved when the surface energy of the polymer was adjusted to be similar to that of $PC_{71}BM$ (34.3 mN m^{-1}). Consequently, the photovoltaic device based on **PIDTDPP3** showed the highest performance of 3.67%

Table 2 Surface energy of polymers and photovoltaic parameters for polymer:$PC_{71}BM$ BHJ devices

Polymer	Surface energy/ mN m^{-1}	BHJ roughness/ nm	V_{oc}/ V	J_{sc}/ mA cm^{-2}	FF (%)	PCE (%)
PIDTDPP1	30.2	4.24	0.77	2.63	0.47	0.95
PIDTDPP2	31.9	3.15	0.78	5.64	0.49	2.16
PIDTDPP3	34.8	0.90	0.76	9.80	0.49	3.67

compared to 0.95% for **PIDTDPP1** due to the more efficient exciton dissociation and charge transport.

Experimental section

Materials and instruments

All chemicals were purchased from Aldrich or TCI and used without further purification, unless otherwise noted. Toluene was distilled from sodium under nitrogen atmosphere using benzophenone as an indicator. *N*,*N*-Dimethylformamide (DMF) was dried over CaH_2 and distilled under vacuum. 3,6-Dithiophen-2-yl-2,5-dihydro-pyrrolo[3,4-*c*]pyrrole-1,4-dione (**1**) and 3,6-bis-(5-bromo-thiophen-2-yl)-2,5-di-2-ethylhexyl-pyrrolo[3,4-*c*]pyrrole-1,4-dione (**4**) were prepared according to the literature.[37] Compound **5** was prepared by our previously reported procedure.[34]

^{1}H and ^{13}C NMR spectra were carried out on Bruker AV 300 or 500 spectrometers operating at 300 or 125 MHz in $CDCl_3$. ESI-MS spectra were obtained using a Bruker APEX Qe 47e Fourier transform (ion cyclotron resonance) mass spectrometer. The gel permeation chromatography (GPC) measurements were performed on a Waters 1515 chromatograph with a refractive index detector at room temperature with THF as an eluent. UV-Vis spectra were recorded using a Perkin-Elmer Lambda-9 spectrophotometer. The differential scanning calorimetry (DSC) tests were studied by a DSC 2010 (TA Instruments) with a heating rate of 10 °C min^{-1} and a nitrogen flow of 50 mL min^{-1}. Cyclic voltammetry (CV) measurements were conducted on a BAS CV-50W voltammetric system with a three-electrode cell in acetonitrile with 0.1 M of tetrabutylammonium hexafluorophosphate using a scan rate of 100 mV s^{-1} with ITO, Ag/AgCl and Pt mesh as the working electrode, reference electrode and counter electrode, respectively. AFM images were recorded on a Veeco multimode AFM with a Nanoscope III controller under tapping mode. Contact angle tests were performed with a VCA Optima Surface Analysis System (Advanced Surface Technology Products, Billerica, MA) and the values are the average of five measurement results per polymer film with a standard deviation of ±3°.

Synthesis

Compound 2. A mixture of 3,6-dithiophen-2-yl-2,5-dihydro-pyrrolo[3,4-*c*]pyrrole-1,4-dione (1.00 g, 3.3 mmol) and anhydrous K_2CO_3 (1.50 g, 10.9 mmol) was dissolved in 40 mL of anhydrous DMF and heated to 120 °C under N_2 for 1 h. To the resulting solution, 1-bromo-6-cyanohexane (1.61 g, 8.5 mmol) was added dropwise and then the mixture was stirred under N_2 at 130 °C for 24 h. After cooling to room temperature, the reaction solution was poured into cold water (300 mL) and extracted with chloroform (3 × 100 mL). The combined organic layers were dried over anhydrous Na_2SO_4 and the solvent was evaporated under vacuum. The residue was further purified on the silica gel column by eluting with chloroform ($CHCl_3$) to afford **2** as a dark red solid (1.14 g, 67%). ^{1}H NMR ($CDCl_3$, ppm): δ 8.93 (d, J = 3.87 Hz, 2H), 7.68 (d, J = 5.01 Hz, 2H), 7.33 (m, 2H), 4.13 (t, J = 7.50 Hz, 4H), 2.38 (t, J = 6.90 Hz, 4H), 1.58–1.87 (m, 8H), 1.27 (m, 4H). ^{13}C NMR ($CDCl_3$, ppm): δ 161.29, 139.91, 135.48, 130.94, 129.46, 128.81, 119.53, 107.61, 41.57, 29.11, 25.83, 24.99, 17.09. HRMS (ESI): (M^+, $C_{26}H_{26}N_4O_2S_2$) calcd 490.1497; found 490.1570.

Compound 3. A solution of **2** (0.52 g, 1 mmol) in $CHCl_3$ (50 mL) was stirred at room temperature (RT) for 2 h under nitrogen before *n*-bromosuccinimide (0.41 g, 2.3 mmol) was added in portions. The mixture was kept in the dark for 24 h and then quenched with methanol (200 mL). The crude solid was collected by vacuum filtration and washed with water and methanol. Following that, the residue was further purified on the silica gel column using $CHCl_3$ as the eluent to afford compound **3** as a dark red solid (0.42 g, 62%). ^{1}H NMR ($CDCl_3$, ppm): δ 8.69 (d, J = 4.17 Hz, 2H), 7.28 (d, J = 4.05 Hz, 2H), 4.05 (t, J = 7.50 Hz, 4H), 2.40 (t, J = 5.70 Hz, 4H), 1.58–1.79 (m, 8H), 1.27 (m, 4H). ^{13}C NMR ($CDCl_3$, ppm): δ 180.21, 163.90, 160.90, 139.01, 135.58, 131.86, 130.62, 119.46, 41.63, 29.72, 29.22, 25.83, 24.98, 17.11. HRMS (ESI): (M^+, $C_{26}H_{24}Br_2N_4O_2S_2$) calcd 645.9707; found 645.9600.

Polymer PIDTDPP1. Compounds **5** (123.4 mg, 0.1 mmol) and **4** (68 mg, 0.1 mmol) were dissolved in anhydrous toluene (5 mL) and DMF (0.5 mL) and the solution was carefully degassed before the addition of $Pd_2(dba)_3$ (4 mg) and P(*o*-tol)$_3$ (10 mg). The resulting solution was heated to 110 °C and stirred under N_2 for 48 h. The reaction mixture was allowed to cool down to RT and subsequently added dropwise into methanol (200 mL). The precipitation was obtained by vacuum filtration and then washed by Soxhlet extraction with acetone and hexane. The solid was then redissolved in chloroform and then precipitated again from hexane. Vacuum filtration and drying afforded the polymer **PIDTDPP1** as a dark black solid (79%). ^{1}H NMR (500 MHz, $CDCl_3$) δ 8.90 (br, 2H), 7.43 (br, 6H), 7.19 (m, 8H), 7.13 (m, 8H), 4.05 (br, 4H), 2.60–2.38 (br, 16H), 1.58–0.89 (m, 62H). M_n = 65.1 kDa, M_w = 148 kDa, PDI = 2.27.

Polymer PIDTDPP2. PIDTDPP2 was prepared from **5** (123.4 mg, 0.1 mmol), **4** (34 mg, 0.05 mmol) and **3** (34 mg, 0.05 mmol) using the same method as for **PIDTDPP1** with a yield of 82%. ^{1}H NMR (500 MHz, $CDCl_3$) δ 8.97–8.90 (br, 2H), 7.43 (br, 6H), 7.20 (m, 8H), 7.10 (m, 8H), 4.05 (br, 4H), 2.59 (br, 12H), 1.92 (br, 4H), 1.58–0.89 (m). M_n = 65.8 kDa, M_w = 192 kDa, PDI = 2.92.

Polymer PIDTDPP3. PIDTDPP3 was prepared from **5** (123.4 mg, 0.1 mmol) and **3** (68 mg, 0.1 mmol) using the same method as **PIDTDPP1** with a yield of 86%. ^{1}H NMR (500 MHz, $CDCl_3$) δ 8.89 (br, 2H), 7.44 (br, 6H), 7.20 (m, 8H), 7.13 (m, 8H), 4.12 (br, 4H), 2.59–2.38 (br, 16H), 1.58–0.89 (m, 52H). M_n = 98 kDa, M_w = 284 kDa, PDI = 2.90.

Fabrication of the OFET device

To fabricate the field-effect transistor, a heavily doped silicon wafer used as the common gate electrode with a 300 nm thick thermally oxidized SiO_2 gate dielectric layer was first cleaned in acetone and isopropanol through sonication and then treated with air plasma. The cleaned substrate was exposed to hexamethyldisilazane (HMDS) in a vacuum oven (200 mTorr, 100 °C) for 3 hours. The wafer was transferred to a nitrogen filled glove box and the polymer film was spin-coated from a 10 mg mL^{-1} chloroform solution which was stirred for 10 h and filtered through a 0.2 μm PTFE filter. Subsequently, a 50 nm thick gold film was evaporated as the interdigitated source and drain electrodes (L = 1000 μm, W = 12 μm) defined through a shadow mask. All the FET device measurements were performed in the glove box using an Agilent 4155B semiconductor parametric analyzer. And the reported values are an average of the results from five different devices.

Photovoltaic device fabrication

To fabricate BHJ polymer solar cells, the PEDOT:PSS (Baytron® PVP AI 4083, filtered at 0.45 μm) layer (~45 nm) was spin-coated onto the pre-cleaned ITO-coated glass substrates (cleaned with detergent, de-ionized water, acetone, and isopropyl alcohol). Then the substrate was baked on a hotplate at 150 °C for 10 min. The BHJ film was spin-coated in a nitrogen filled glove box from an *o*-DCB solution of polymer/$PC_{71}BM$, which was pre-stirred overnight and filtered through a 0.2 μm PTFE filter. Subsequently, calcium (30 nm) and aluminium (100 nm) were thermally evaporated on top of the active layer sequentially under high vacuum (<2 × 10^{-7} Torr) with a shadow mask to define the active area of the devices (10.08 mm^2). Device testing was carried out in a glove box with a Keithley 2400 SMU source measurement unit and an Oriel xenon lamp (450 W) using an AM 1.5 filter as the solar simulator. The device results have been calibrated by a standard silicon solar cell with a KG5 filter.

Acknowledgements

This work has been supported by the National Science Foundation's NSF-STC program under grant no. DMR-0120967, the AFOSR (FA9550-09-1-0426), the Office of Naval Research (N00014-11-1-3000), and the World Class University (WCU) program through the National Research Foundation of Korea under the Ministry of Education, Science and Technology (R31-21410035). A.K.-Y.J. thanks for the financial support of the Boeing-Johnson Foundation. Y. Sun thanks the State-Sponsored Scholarship for Graduate Students from China Scholarship Council. S. C. Chien thanks the National Science Council of Taiwan (NSC98-2917-I-009-112) for supporting the Graduate Students Study Abroad Program.

Notes and references

1 H. Y. Chen, J. H. Hou, S. Q. Zhang, Y. Y. Liang, G. W. Yang, Y. Yang, L. P. Yu, Y. Wu and G. Li, *Nat. Photonics*, 2009, **3**, 649.
2 Y. Y. Liang, D. Q. Feng, Y. Wu, S. T. Tsai, G. Li, C. Ray and L. P. Yu, *J. Am. Chem. Soc.*, 2009, **131**, 7792.
3 Y. Y. Liang, Z. Xu, J. B. Xia, S. T. Tsai, Y. Wu, G. Li, C. Ray and L. P. Yu, *Adv. Mater.*, 2010, **22**, E135.
4 S. C. Price, A. C. Stuart, L. Yang, H. Zhou and W. You, *J. Am. Chem. Soc.*, 2011, **133**, 4625.
5 T.-Y. Chu, J. Lu, S. Beaupré, Y. Zhang, J.-R. m. Pouliot, S. Wakim, J. Zhou, M. Leclerc, Z. Li, J. Ding and Y. Tao, *J. Am. Chem. Soc.*, 2011, **133**, 4250.
6 H. J. Son, W. Wang, T. Xu, Y. Liang, Y. Wu, G. Li and L. Yu, *J. Am. Chem. Soc.*, 2011, **133**, 1885.
7 Y. Zhang, J. Zou, H.-L. Yip, Y. Sun, J. A. Davies, K.-S. Chen, O. Acton and A. K. Y. Jen, *J. Mater. Chem.*, 2011, **21**, 3895.
8 Y. Sun, M. Wang, X. Gong, J. H. Seo, B. B. Y. Hsu, F. Wudl and A. J. Heeger, *J. Mater. Chem.*, 2011, **21**, 1365.
9 Z. He, C. Zhong, X. Huang, W.-Y. Wong, H. Wu, L. Chen, S. Su and Y. Cao, *Adv. Mater.*, 2011, **23**, 4636.
10 B. C. Thompson and J. M. J. Frechet, *Angew. Chem., Int. Ed.*, 2008, **47**, 58.
11 L. M. Chen, Z. R. Hong, G. Li and Y. Yang, *Adv. Mater.*, 2009, **21**, 1434.
12 J. Peet, M. L. Senatore, A. J. Heeger and G. C. Bazan, *Adv. Mater.*, 2009, **21**, 1521.
13 H. Zhou, L. Yang, A. C. Stuart, S. C. Price, S. Liu and W. You, *Angew. Chem., Int. Ed.*, 2011, **50**, 2995.
14 C. J. Brabec, M. Heeney, I. McCulloch and J. Nelson, *Chem. Soc. Rev.*, 2011, **40**, 1185.
15 T. M. Clarke and J. R. Durrant, *Chem. Rev.*, 2010, **110**, 6736.
16 J. E. Slota, X. He and W. T. S. Huck, *Nano Today*, 2010, **5**, 231.
17 J. Peet, J. Y. Kim, N. E. Coates, W. L. Ma, D. Moses, A. J. Heeger and G. C. Bazan, *Nat. Mater.*, 2007, **6**, 497.
18 J. K. Lee, W. L. Ma, C. J. Brabec, J. Yuen, J. S. Moon, J. Y. Kim, K. Lee, G. C. Bazan and A. J. Heeger, *J. Am. Chem. Soc.*, 2008, **130**, 3619.
19 T. Salim, L. H. Wong, B. Brauer, R. Kukreja, Y. L. Foo, Z. Bao and Y. M. Lam, *J. Mater. Chem.*, 2011, **21**, 242.
20 S. T. Zhang, Z. J. Wang, J. M. Zhao, Y. Q. Zhan, Y. Wu, Y. C. Zhou, X. M. Ding and X. Y. Hou, *Appl. Phys. Lett.*, 2004, **84**, 2916.
21 M. Helgesen, S. A. Gevorgyan, F. C. Krebs and R. A. J. Janssen, *Chem. Mater.*, 2009, **21**, 4669.
22 Y. Zhang, S.-C. Chien, K.-S. Chen, H.-L. Yip, Y. Sun, J. A. Davies, F.-C. Chen and A. K. Y. Jen, *Chem. Commun.*, 2011, **47**, 11026.
23 J. T. Henssler, X. Zhang and A. J. Matzger, *J. Org. Chem.*, 2009, **74**, 9112.
24 J. S. Kim, Y. Lee, J. H. Lee, J. H. Park, J. K. Kim and K. Cho, *Adv. Mater.*, 2010, **22**, 1355.
25 H. Bronstein, Z. Y. Chen, R. S. Ashraf, W. M. Zhang, J. P. Du, J. R. Durrant, P. S. Tuladhar, K. Song, S. E. Watkins, Y. Geerts, M. M. Wienk, R. A. J. Janssen, T. Anthopoulos, H. Sirringhaus, M. Heeney and I. McCulloch, *J. Am. Chem. Soc.*, 2011, **133**, 3272.
26 C. H. Woo, P. M. Beaujuge, T. W. Holcombe, O. P. Lee and J. M. J. Frechet, *J. Am. Chem. Soc.*, 2010, **132**, 15547.
27 J. C. Bijleveld, A. P. Zoombelt, S. G. J. Mathijssen, M. M. Wienk, M. Turbiez, D. M. de Leeuw and R. A. J. Janssen, *J. Am. Chem. Soc.*, 2009, **131**, 16616.
28 J. C. Bijleveld, V. S. Gevaerts, D. Di Nuzzo, M. Turbiez, S. G. J. Mathijssen, D. M. de Leeuw, M. M. Wienk and R. A. J. Janssen, *Adv. Mater.*, 2010, **22**, E242.
29 Y. N. Li, P. Sonar, S. P. Singh, M. S. Soh, M. van Meurs and J. Tan, *J. Am. Chem. Soc.*, 2011, **133**, 2198.
30 P. Sonar, S. P. Singh, Y. Li, M. S. Soh and A. Dodabalapur, *Adv. Mater.*, 2010, **22**, 5409.
31 T. L. Nelson, T. M. Young, J. Y. Liu, S. P. Mishra, J. A. Belot, C. L. Balliet, A. E. Javier, T. Kowalewski and R. D. McCullough, *Adv. Mater.*, 2010, **22**, 4617.
32 J. C. Bijleveld, V. S. Gevaerts, D. Di Nuzzo, M. Turbiez, S. G. J. Mathijssen, D. M. de Leeuw, M. M. Wienk and R. A. J. Janssen, *Adv. Mater.*, 2010, **22**, E242.
33 Y. Sun, S.-C. Chien, H.-L. Yip, Y. Zhang, K.-S. Chen, D. F. Zeigler, F.-C. Chen, B. Lin and A. K. Y. Jen, *J. Mater. Chem.*, 2011, **21**, 13247.
34 Y. Zhang, J. Zou, H.-L. Yip, K.-S. Chen, D. F. Zeigler, Y. Sun and A. K. Y. Jen, *Chem. Mater.*, 2011, **23**, 2289.
35 Y. Zhang, S. K. Hau, H. L. Yip, Y. Sun, O. Acton and A. K. Y. Jen, *Chem. Mater.*, 2010, **22**, 2696.
36 Y. J. Cheng, S. H. Yang and C. S. Hsu, *Chem. Rev.*, 2009, **109**, 5868.
37 A. B. Tamayo, M. Tantiwiwat, B. Walker and T. Q. Nguyen, *J. Phys. Chem. C*, 2008, **112**, 15543.

38 A. Pivrikas, N. S. Sariciftci, G. Juška and R. Österbacka, *Progress in Photovoltaics: Research and Applications*, 2007, vol. 15, p. 677.
39 Y. Shirota and H. Kageyama, *Chem. Rev.*, 2007, **107**, 953.
40 J. S. Kim, Y. Lee, J. H. Lee, J. H. Park, J. K. Kim and K. Cho, *Adv. Mater.*, 2010, **22**, 1355.
41 X. Bulliard, S.-G. Ihn, S. Yun, Y. Kim, D. Choi, J.-Y. Choi, M. Kim, M. Sim, J.-H. Park, W. Choi and K. Cho, *Adv. Funct. Mater.*, 2010, **20**, 4381.
42 M. Geoghegan and G. Krausch, *Prog. Polym. Sci.*, 2003, **28**, 261.